Solid Freeform Fabrication 2016: Proceedings of the 27th Annual International Solid Freeform Fabrication Symposium – An Additive Manufacturing Conference
Reviewed Paper

An Investigation of the Dendritic Segregation in Single-Crystal René N5 Fabricated Through Scanning Laser Epitaxy

Amrita Basak[1], and Suman Das[1, 2]

[1]George W. Woodruff School of Mechanical Engineering, 813 Ferst Dr NW, Georgia Institute of Technology, Atlanta, GA 30332
[2]School of Materials Science and Engineering, Georgia Institute of Technology, 771 Ferst Dr NW, Atlanta, GA 30313

Keywords: Additive Manufacturing, Scanning Laser Epitaxy, Nickel-base, Superalloys, René N5, Elemental Segregation

Abstract

Dendritic segregation in single-crystal nickel-base superalloy René N5 was investigated in the present study. Samples of René N5 were fabricated through scanning laser epitaxy (SLE) process. SLE is a metal powder bed fusion-based additive manufacturing (AM) process that was exclusively developed for the repair and manufacture of gas turbine hot-section components using nickel-base superalloys. The concentration profiles of the alloying elements in the SLE fabricated René N5 samples obtained from the energy dispersive X-ray spectroscopy (EDS) measurements exhibited strong segregation of rhenium (Re) and tungsten (W) in the dendrite cores, and aluminum (Al) and tantalum (Ta) in the interdendritic regions. Carbides were found to be rich in tantalum (Ta) and tungsten (W). However, a trace amount of rhenium (Re) was also found in the carbide precipitates. In the final stages of the solidification tungsten (W) showed a tendency to accumulate in a γ phase layer around the eutectic pool. This work is sponsored by the Office of Naval Research through grants N00014-14-1-0658.

Introduction

Nickel-base superalloys are extensively used for the manufacture of hot-section components of gas turbines as this class of alloys offer higher yield strength with increasing operating temperatures primarily due to the presence of the secondary phases. The secondary phases form an antiphase boundary and lock the associated dislocation movements. Superalloys develop high-temperature strength through solid-solution-strengthening as well as precipitation-strengthening mechanisms. Thus, the properties of the nickel-base superalloys can be tailored through the addition of various elements that can alter the precipitation kinetics. The secondary phase precipitates such as γ′ and carbides are typically formed through precipitation mechanisms. Aluminum and titanium promote precipitation of the γ′ phases. Chromium, iron, cobalt, molybdenum, and rhenium all preferentially partition to the γ matrix while aluminum, titanium, niobium, tantalum, and vanadium preferentially partition to the γ′ precipitates and strengthen the matrix through solid-solution and precipitates. Boron and zirconium tend to segregate to the grain boundaries. Such segregation reduces the grain boundary energy and results in better grain boundary cohesion and ductility. Another form of grain boundary strengthening is achieved through the addition of carbon and a carbide former, such as chromium, molybdenum, tungsten,

niobium, tantalum, titanium, or hafnium. The carbide formers drive precipitation of carbides at the grain boundaries and such precipitation reduces grain boundary sliding.

The gas turbine hot-section components are increasingly being cast with directionally-solidified (DS) or single-crystal (SX) microstructures to further improve the physical, mechanical and thermal properties. The first generation SX superalloys typically have 8-10 wt. % Cr, 4-11 wt. % tungsten (W), and no rhenium (Re). The second generation SX superalloys typically have 5-8 wt. % Cr, 5-8 wt. % W and 3 wt. % Re. The second generation SX superalloys have successfully been applied in various commercial and military aircraft engines. René N5 is a rhenium containing second-generation SX superalloy developed at General Electric. The presence of rhenium delays coarsening of the γ′ phase, and increases γ/γ′ misfit [1]. René N5 is also strengthened by the solid-solution-strengthening effects of chromium (Cr), tantalum (Ta) and tungsten (W). Aluminum (Al) and titanium (Ti) provide additional strength due to the precipitation-hardening effects of the γ′ phase. Although the γ′ phase is the main reason for improvements in the thermo-mechanical properties, it also increases the processing difficulties in terms of manufacturing and repair as these alloys are prone to crack formation and, therefore, expensive to cast and weld [2].

Research on additive manufacturing-based repair and manufacture of SX superalloys is still in its infancy. Epitaxial laser metal forming (ELMF) was the first AM process to demonstrate the formation of multiple layers of SX CMSX-4® [3]. Similar results were also achieved for dissimilar material systems such as Ni-Cr-Al-Y [4] and M-Cr-Al-Y [5]. Single-crystal deposits of René N4 were produced using direct metal deposition (DMD) process [6]. Electron beam melting (EBM) process was applied to René 142 powders for the fabrication of DS deposits [7]. CMSX-4® powder was also processed through EBM process [8, 9]. The SLE process has shown significant potential for one step repair of single-crystal CMSX-4® [10-12]; equiaxed René 80 [13], and equiaxed IN100 [14]. A major concern in the single-crystal superalloy development is the formation of defects during unidirectional solidification. Strong partitioning tendency of high-density refractory elements such as W, Re, and Ta affect the thermosolutal convection. Such convection leads to density inversion in the mushy zone. During unidirectional solidification in conventional casting furnaces, the density inversion may lead to the formation of unacceptable grain defects or freckles. Chemistry optimization is, therefore, necessary to establish an optimum content of refractory elements (Ta, Re, W) in order to reduce defects. The high segregation of some alloying elements in superalloys can be diminished by expensive high-temperature homogenization heat treatments.

In the present study, samples of René N5 were fabricated through scanning laser epitaxy (SLE) process through a single-pass deposition utilizing powder beds of thicknesses exceeding 1000 μm. The dendritic microstructures of the deposits were investigated through optical microscopy, scanning electron microscopy (SEM), and energy dispersive X-ray spectroscopy (EDS). A quantitative description of the segregation of the various elements in SX was obtained using EDS measurements. The EDS measurements were used to determine the partition coefficients for the elements of the multicomponent alloys. Three different partition coefficients were defined to accurately measure the level of elemental segregation. These partition coefficients were between the dendrite core and the interdendritic region, between the

interdendritic region and the eutectic pools, and between the interdendritic region and the carbides.

Materials and Methods

The nickel-base superalloy René N5 was chosen in this work. The René N5 powder was produced by Praxair Surface Technologies using an atomization process. The composition of the René N5 powder is given in Table I. Hf (0.15 wt. %), C (0.05 wt. %) and B (0.004 wt. %) were also found in trace quantities. The morphology and the cross-section of powder were analyzed using optical microscopy and scanning electron microscopy (SEM). The René N5 powders are mostly spherical, although some irregularity in shape is found as shown in Fig. 1(a). The powder was mounted in Bakelite and polished to a mirror finish. The cross-section was analyzed under an optical microscope for the inspection of internal porosity, and limited internal porosity was detected as shown in Fig. 1(b).

Table I. Composition of the René N5 powder (wt. %).

	Cr	Co	Mo	Re	W	Al	Ta	Ni
René N5	7.1	8.0	2.0	3.0	5.0	6.0	7.0	Bal

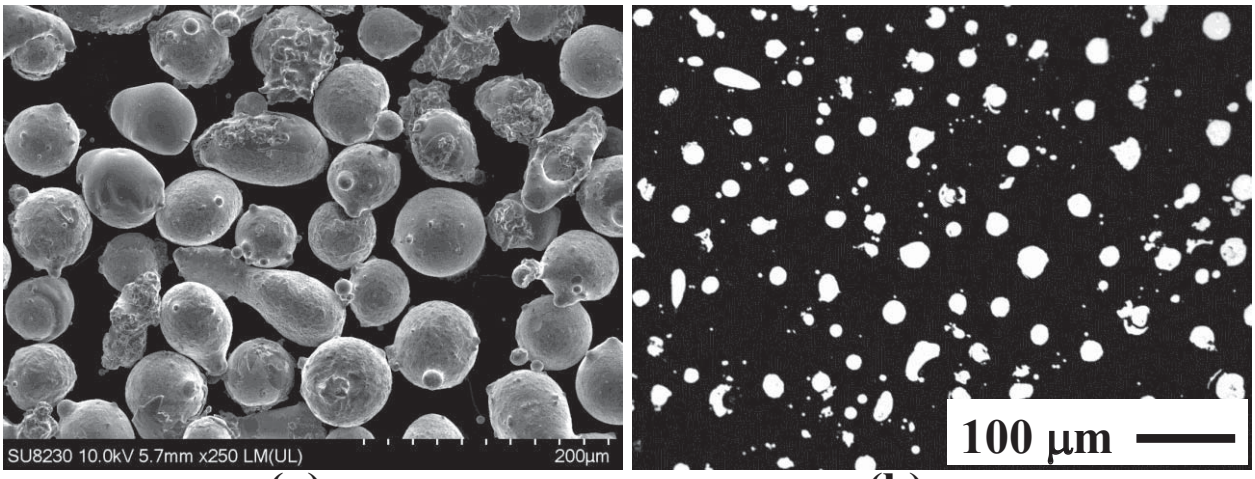

Figure 1. (a) SEM image of the René N5 powder and (b) optical microscopic image of the René N5 powder cross-section after polishing.

SLE processed samples were sectioned along the length and width for the inspection of the microstructure. A Buehler automated saw was used to cut the samples. Each section is mounted in Bakelite and polished to a mirror finish; starting with 80 grit paper and progressively increasing the size to 1200 grit. The samples were then rough-polished using 5 µm and 3 µm diamond solutions. Finally, the samples were fine polished using a 0.5 µm colloidal alumina suspension. The polished samples were then etched with Marble's reagent (50 ml HCl, 50 ml H_2O, and 10.0 gm $CuSO_4$) to eliminate the γ' phase and reveal the dendritic microstructure. A Leica DM6000 optical microscope was thereafter used to take the images. The microstructural investigation of the SLE processed René N5 was carried out on a Hitachi SU8230 SEM.

Elemental analysis was carried out using energy dispersive X-ray spectroscopy (EDS) on the Hitachi SU8230 (with Oxford Instruments Aztec Energy EDX system).

Experimental Procedure

The SLE process was conducted on rectangular SX cast René N5 coupons having dimensions of 35.56 mm X 6.86 mm X 2.54 mm. Each substrate was placed into a 35.56 mm x 6.86 mm recess cut into an IN625 base plate. The powder was placed above the substrate using rectangular wells cut into an Aluminum mask plate. Once the samples were prepared, they were placed into an atmospheric process chamber that is purged with high purity (99.999%) Argon. A 1kW Ytterbium fiber laser (IPG Photonics, Model: YLS-1000) was used with a Cambridge Technologies galvanometer scanner to focus the beam on top of the substrate. A raster scan pattern across the width of the sample generated a melt pool that linearly traveled along the length of the substrate.

Results and Discussions

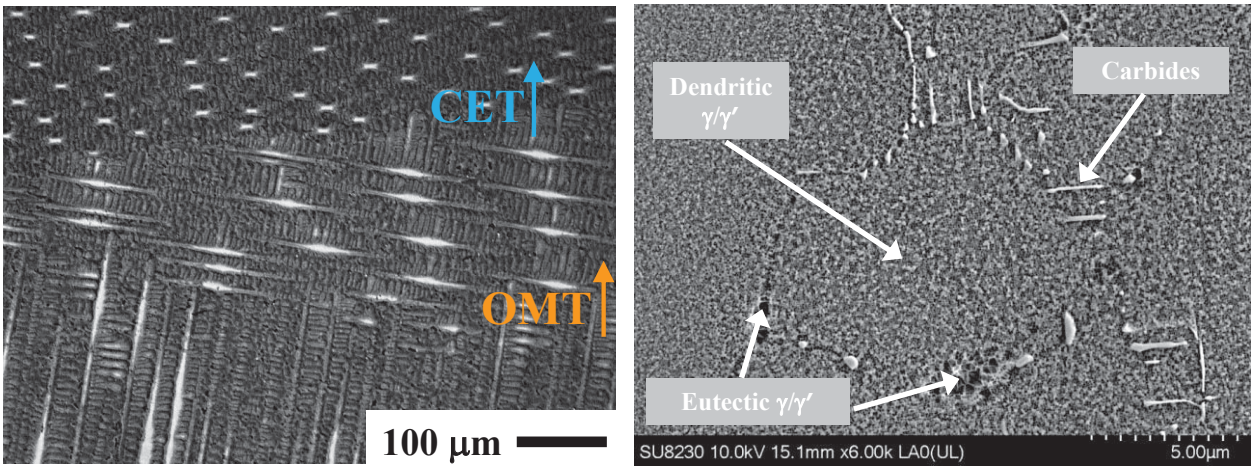

Figure 2. Representative transverse optical micrograph of René N5 sample the oriented-to-misoriented transition (OMT) and the columnar-to-equiaxed transition (CET) and (b) SEM image showing the γ matrix, the γ' precipitates in the γ matrix, the eutectics and the carbides.

The as-deposited single-crystal René N5 exhibited a dendritic microstructure typically observed in directionally solidified or single-crystal alloys as shown in Fig. 2(a). A detailed view of the SX growth transition from the <001> to the <100> direction can also be seen in Fig. 2(a). This change is known as the oriented-to-misoriented transition (OMT). The OMT was caused by a change in direction of the dominant temperature gradient as the substrate became increasingly hot toward the end of the scan. Figure 2(a) also provides a detailed view of the transition from the columnar-to-equiaxed morphology, known as the CET. A constitutionally undercooled zone was formed due to the increase in isotherm velocity near the surface and the decrease in the temperature gradient resulting in the CET. The high degree of elemental segregation from the dendrite cores to the interdendritic regions is clearly visible. Due to the segregation of heavy

elements such as W and Re at the core of dendrite and enrichment of light elements such as the Al and Ta in the interdendritic region, the dendritic region appears bright and the interdendritic region appears gray after etching as illustrated in Fig. 2(a). The major constituents of the microstructure of René N5 are the γ matrix, the γ' precipitates in the γ matrix, the eutectics, and the carbides. Figure 2(b) illustrates an SEM image of the deposit region showing the major constituents. Fine-scale carbides were formed within the interdendritic regions.

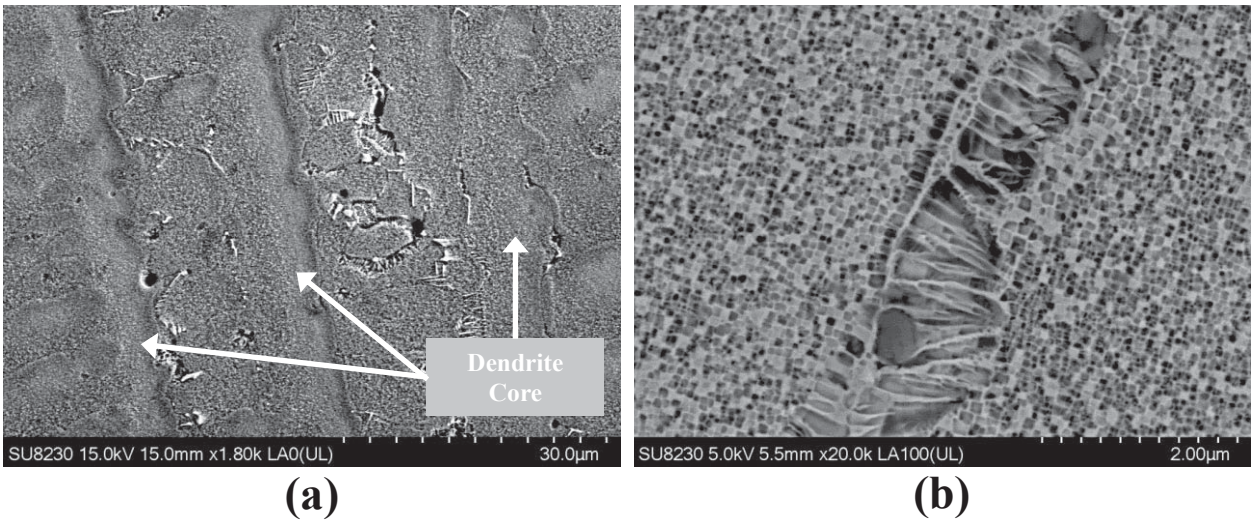

Figure 3. SEM image showing (a) dendritic morphology and (b) the morphologies of the γ/γ' phases in the eutectic regions.

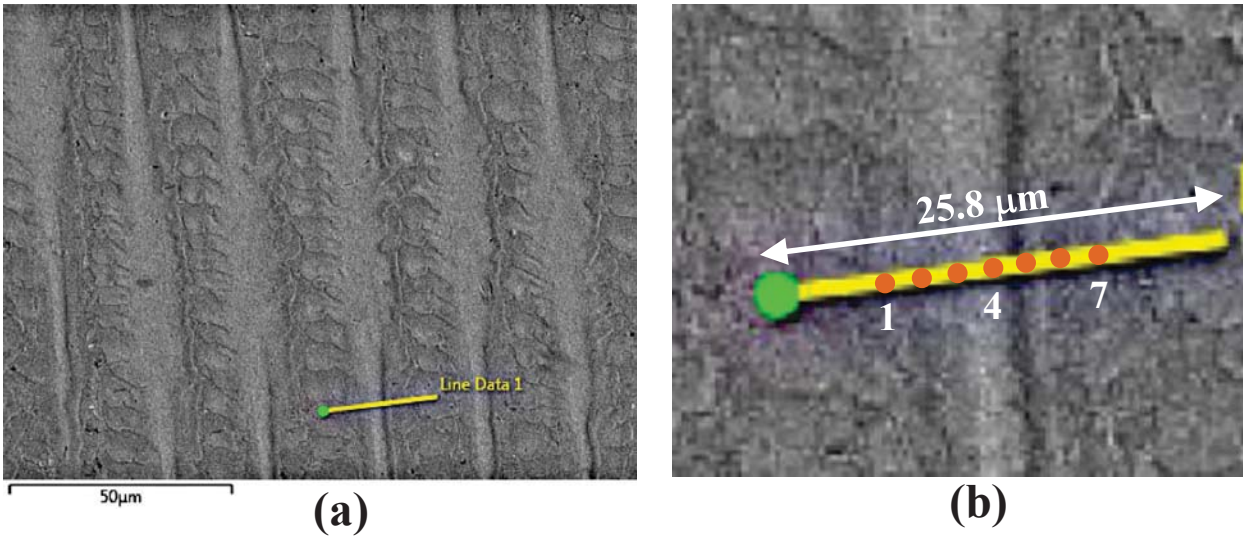

Figure 4. (a) SEM image showing the location of EDS line scan, and (b) zoomed view of the line scan domain illustrating the locations in Figs. 5(a) through 5(i).

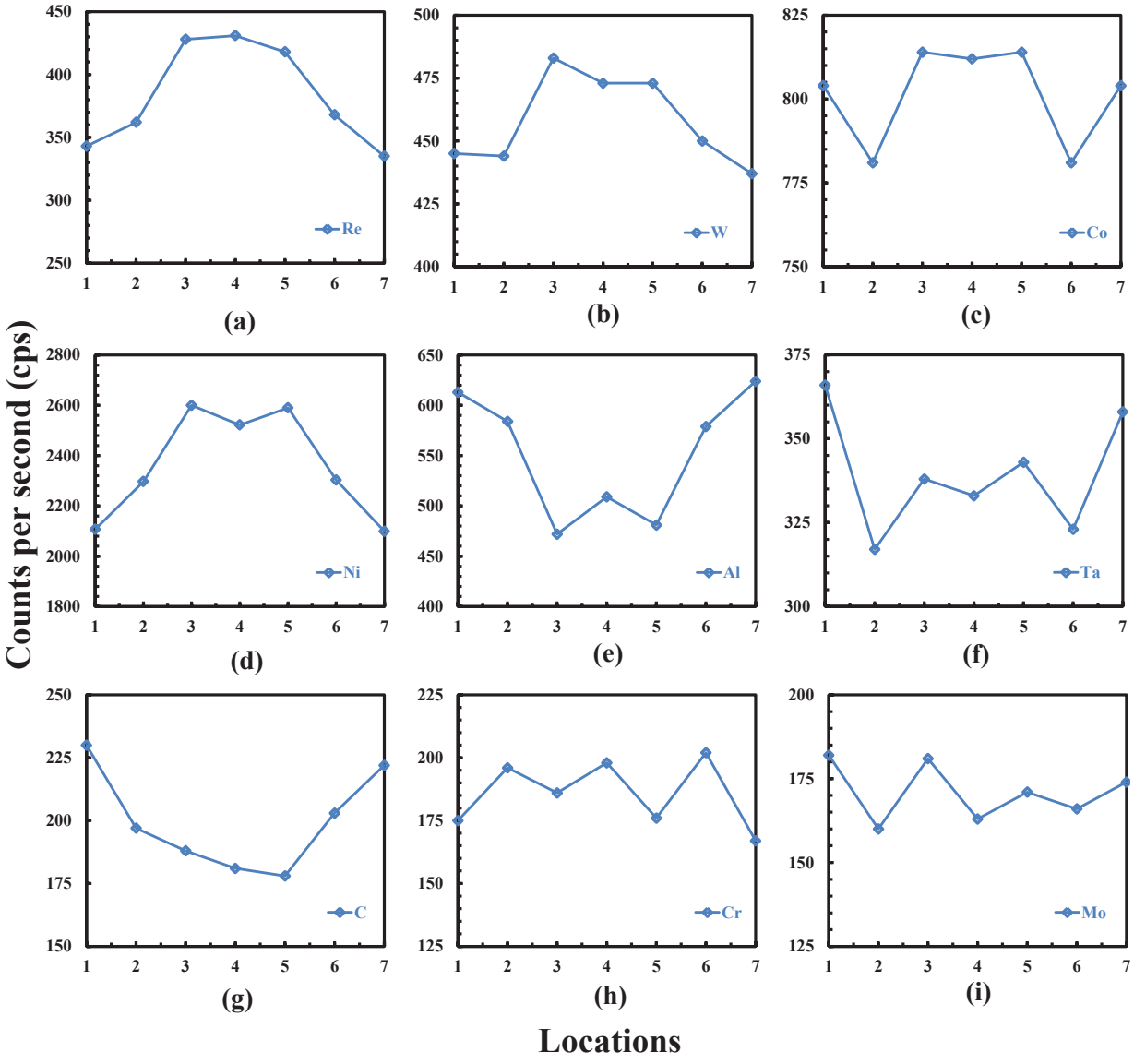

Figure 5. SEM-EDS concentration profiles for various elements in the dendritic core of the SLE deposited René N5.

During unidirectional solidification, γ-dendrites with orientations close to the <001> crystallographic direction grew from the liquid approximately along the direction of the dominant thermal gradient as shown in Fig. 3(a). The dendritic core can be clearly seen in Fig. 3(a) along with the secondary dendritic arms originating from the primary dendritic cores. The interdendritic regions showed coarse γ/γ′ structures compared to the dendritic cores. The interdendritic region was also abundant with carbide precipitates. Figure 3(b) illustrates the γ/γ′ morphology in the eutectic region. Typically, the γ′ forming elements e.g. Al, Ta etc. enrich in the melt, while the elements W and Re are enriched in the dendrites. Thus, as solidification progresses towards the final stage, γ′ starts to form large precipitates in the interdendritic regions. These are commonly called the eutectic islands or eutectics. The microstructures in Fig. 3(b) show the cubic and the channel shaped γ/γ′ precipitates in the eutectic region. Figure 3(b) also

shows the complex tree-root like γ/γ′ structures in the eutectic regions. The partition of the alloying elements at the solid-liquid (S/L) interface and the reduced solid diffusivity of the heavy refractory elements generate highly segregated structures.

EDS line scan measurements were performed across a representative dendrite core as shown in Fig. 4(a). The line data was analyzed and the values were extracted at locations 1 through 7 as shown in Fig. 4(b). The EDS concentration (in cps) profiles are shown in Figs. 5(a) through 5(i). The refractory elements (Re, W) were present in higher quantities in the dendrite cores than in the interdendritic regions as shown in Figs. 5(a) and 5(b), respectively. The γ forming elements, Ni, and Co exhibited higher concentrations in the dendritic region by preferentially partitioning to the γ matrix as shown in Figs. 5(c) and 5(d) respectively. However, the γ' forming elements (Al, Ta) exhibited an opposite behavior, showing higher concentrations in the interdendritic regions as shown in Figs. 5(e) and 5(f). EDS scan results also revealed that C strongly segregated in the interdendritic region as shown in Fig. 5(g). The higher concentration of C and refractory elements in the interdendritic region formed various grain boundary precipitates such as carbides resulting in an improvement in grain boundary ductility and cohesion. Cr and Mo did not show any segregation behavior as shown in Figs. 5(h) and 5(i).

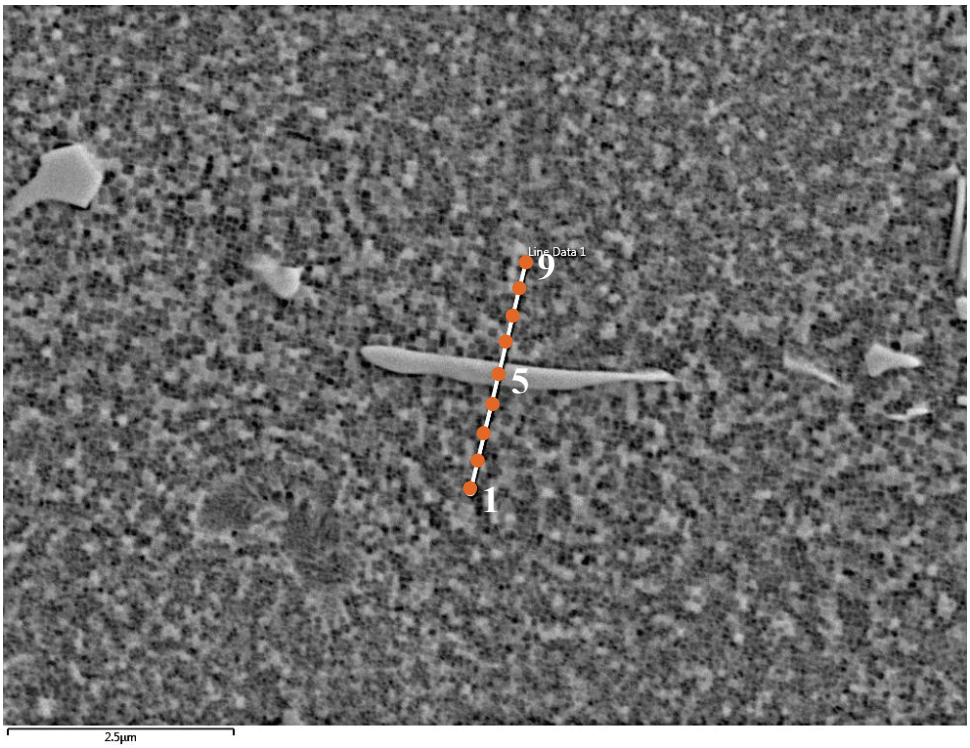

Figure 6. SEM image illustrating the EDS line scan showing the locations in Figs. 7(a) through 7(i).

EDS line scan measurements were performed across a representative carbide precipitate as shown in Fig. 6. The line data was analyzed and the values were extracted at locations 1 through 9 as shown in Fig. 6. Figures 7(a) through 7(i) illustrate the EDS line scan results for a

carbide precipitate. The refractory elements (Ta, W) were present in higher quantities in the carbides than in the interdendritic regions as shown in Figs. 7(a) and 7(b). Other refractory elements such as Re and Hf were also present in significant quantities in the carbides as shown in Figs. 7(c) and 7(d) respectively. Mo showed weak partition behavior in the carbides as shown in Fig. 7(e). The γ/γ' forming elements such as Ni, Al, Cr, and Co exhibited an opposite behavior, showing higher concentrations in the interdendritic regions as shown in Figs. 7(f) through 7(h). C, as expected, showed higher concentrations in the carbide precipitates (Fig. 7(i)). René N5 contains about 0.004 wt. % of B. Line scan measurements showed an insignificant partitioning behavior for this element between the interdendritic region and the carbide precipitates.

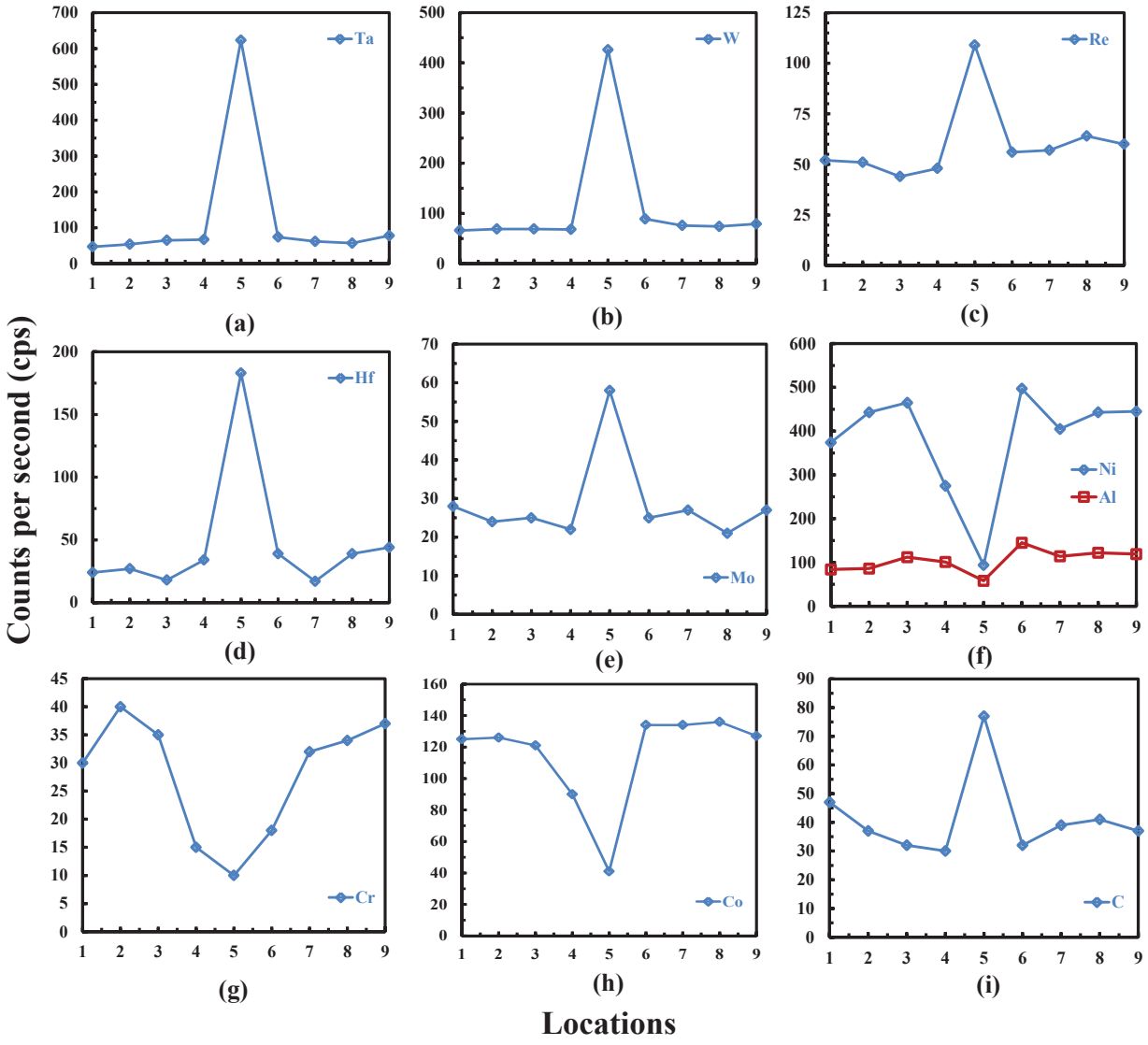

Figure 7. SEM-EDS concentration profiles in the carbide precipitates for various elements in the SLE deposited René N5.

Figure 8 illustrate a typical eutectic region across which an EDS line scan measurement was performed. The line data was analyzed and the values were extracted at locations 1 through

6 as shown in Fig. 8. In cast single-crystal morphologies, the eutectics are typically of order 15-20 μm in size. However, in the SLE fabricated single-crystal morphologies, the eutectics were of order 1-3 μm. Complex eutectics were observed in the SLE fabricated René N5 as shown in Fig. 8. The eutectic γ/γ' was surrounded by the coarse γ/γ' microstructure. A thick γ boundary was found to separate the eutectic γ/γ' and the coarse γ/γ' as shown in Fig. 8.

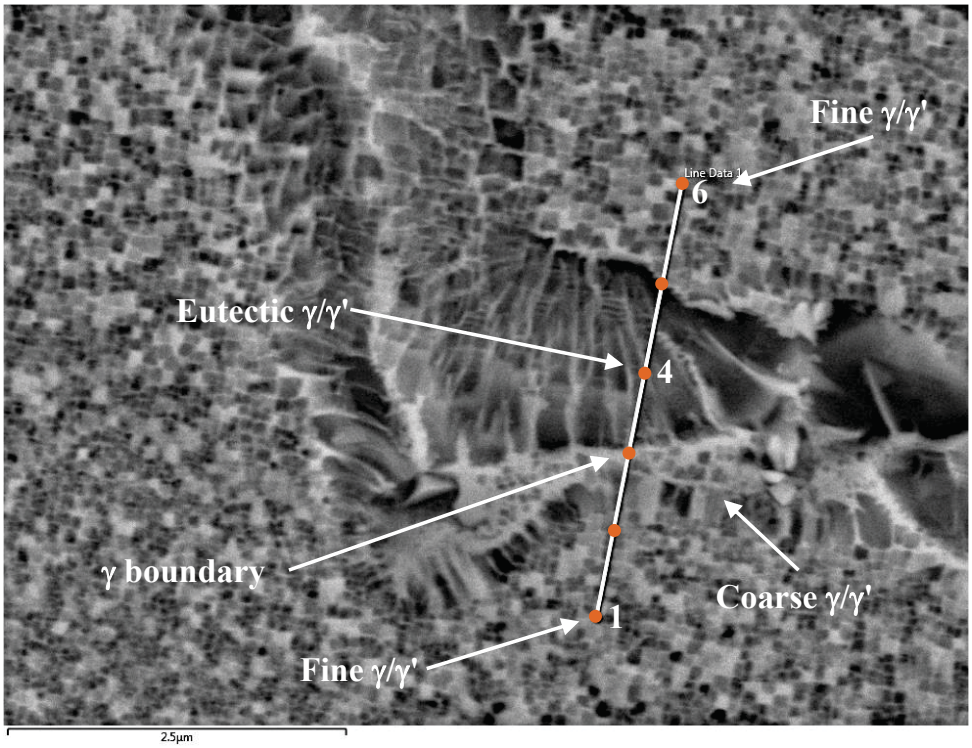

Figure 8. SEM image illustrating the EDS line scan showing the locations in Figs. 9(a) through 9(i).

As shown in Fig. 9(a), Ni and Al were depleted in the eutectic pools (location 4 in Fig. 8) compared to the interdendritic region. Cr showed the highest concentration in the γ layer (location 3 in Fig. 8) around the eutectic. Because the eutectic pools were depleted in Cr, the enrichment of the surrounding layer can occur only if, in the final stages, the interdendritic region solidified first and rejected Cr into the last fraction of liquid. W, Re, Ta, and Hf were also depleted in the eutectic pools as shown in Figs. 9(c) through 9(f). W and Re showed highest concentration in the γ layer (location 3 in Fig. 8) around the eutectic. C strongly segregated to the eutectic as shown in Fig. 9(g). Mo and Co were also found to segregate to the eutectic pool (Fig. 9(h) and 9(i)).

The partition coefficients for various elements were calculated. Three different partition coefficients were defined to accurately measure the level of elemental segregation. These partition coefficients were between the dendrite core and the interdendritic region (k_{DI}), between the eutectic pools and the interdendritic region (k_{EI}), and between the carbides and the interdendritic region (k_{CI}). Table I summarizes the various partition coefficients. The results showed strong segregation tendency of heavy elements (Re, W) to the dendrite core. Ta, W, Re,

Hf, Mo, and C exhibited strong segregation to the carbides. Other elements (Ni, Mo, Co, Cr) exhibited a moderate tendency to partition either to the dendrites or to the interdendritic areas.

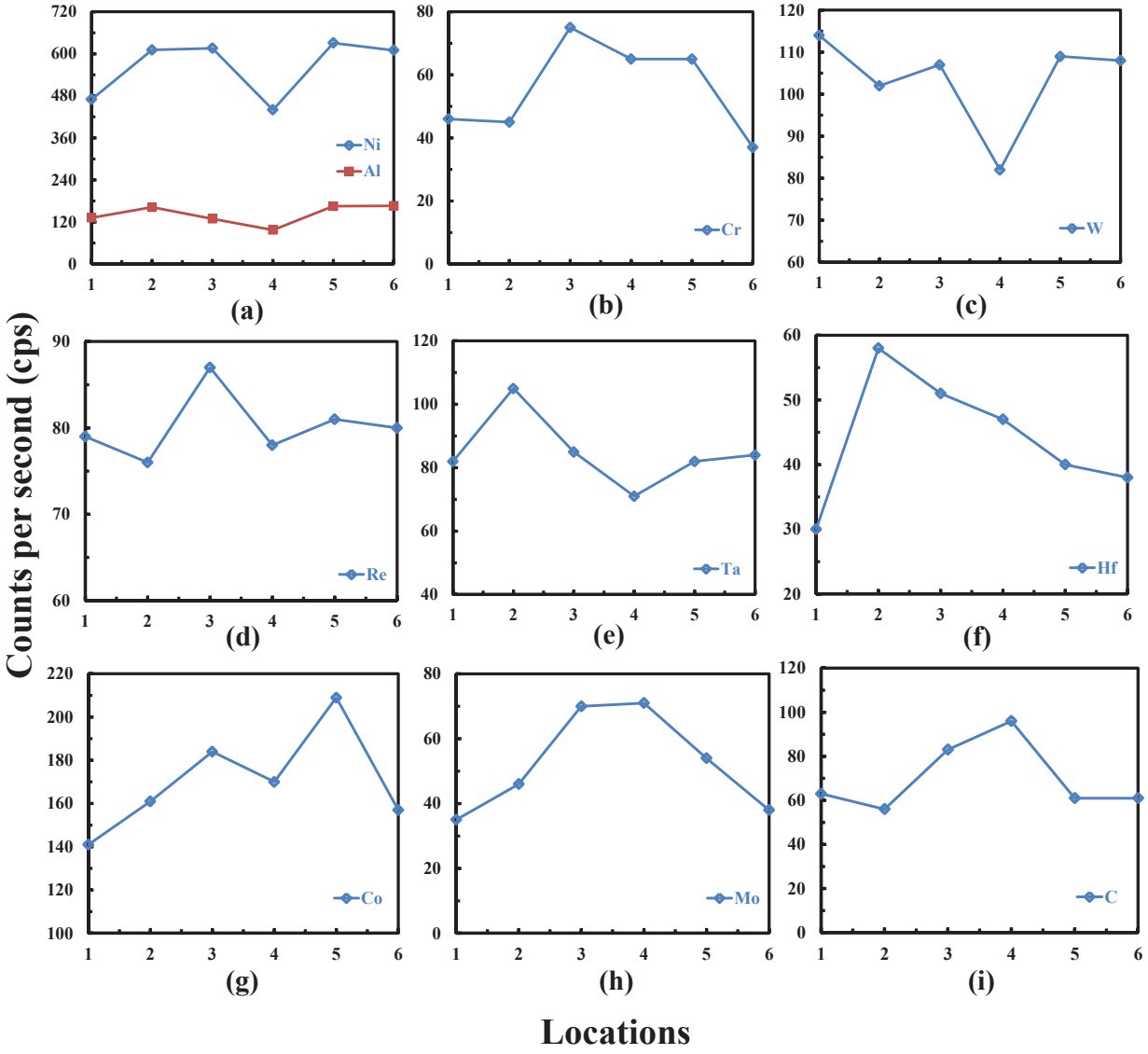

Figure 9. SEM-EDS concentration profiles in the eutectic pools for various elements in the SLE deposited René N5.

Table I. Calculated Partition Coefficients from EDS Results for René N5.

	Al	Ni	C	Cr	Co	Mo	W	Ta	Hf	Re
k_{DI}	0.83	1.20	0.79	1.13	1.01	0.90	1.06	0.91	-	1.26
k_{EI}	0.73	0.94	1.52	1.41	1.21	2.03	0.72	0.87	1.57	0.99
k_{CI}	0.25	0.69	1.64	0.33	0.33	2.07	6.45	13.26	7.63	2.10

Conclusions

In the present study, samples of René N5 were fabricated through the scanning laser epitaxy (SLE) process. The partition coefficients were calculated based on SEM-EDS analysis. The results exhibited a strong segregation tendency of heavy elements (Re, W) to the dendrite core. Interdendritic regions mostly consisted of the γ' forming elements (Al, Mo, and Ta) and carbon (C). In the interdendritic region, Ta, Hf, Re, Mo, W, and C showed strong segregation tendency to the carbide precipitates. In the final stages of solidification, a highly segregated supersaturated γ' phase rich in Cr, Co, and Mo formed a layer around the eutectic pools. Further investigation will be carried out in the future to characterize the effects of heat-treatment on the elemental segregation. A Scheil type of analysis will also be performed to compare the results obtained from the EDS analysis to the theoretical predictions.

Acknowledgments

This work is sponsored by the Office of Naval Research through grant N00014-14-1-0658.

Disclosures

Dr. Suman Das is a cofounder of DDM Systems, a start-up company commercializing SLE technology. Dr. Das and Georgia Tech are entitled to royalties derived from DDM Systems' sale of products related to the research described in this paper. This study could affect their personal financial status. The terms of this arrangement have been reviewed and approved by Georgia Tech in accordance with its conflict of interest policies.

References

[1] Giamei A, Pearson D, Anton D. γ/γ′: The Key to Superalloy Behavior. MRS Proceedings: Cambridge Univ Press; 1984. p. 293.
[2] Sengupta A, Putatunda S, Bartosiewicz L, Hangas J, Nailos P, Peputapeck M, et al. Tensile behavior of a new single-crystal nickel-based superalloy (CMSX-4) at room and elevated temperatures. Journal of Materials Engineering and Performance 1994;3:73-81.
[3] Gäumann M, Henry S, Cleton F, Wagniere J-D, Kurz W. Epitaxial laser metal forming: analysis of microstructure formation. Materials Science and Engineering: A 1999;271:232-41.
[4] Vilar R, Santos E, Ferreira P, Franco N, Da Silva R. Structure of NiCrAlY coatings deposited on single-crystal alloy turbine blade material by laser cladding. Acta Materialia 2009;57:5292-302.
[5] Bezencon C, Schnell A, Kurz W. Epitaxial deposition of MCrAlY coatings on a Ni-base superalloy by laser cladding. Scripta Materialia 2003;49:705-9.
[6] Santos EC, Kida K, Carroll P, Vilar R. Optimization of laser deposited Ni-based single crystal superalloys microstructure. Advanced Materials Research: Trans Tech Publ; 2011. p. 1405-14.
[7] Murr L. Metallurgy of additive manufacturing: Examples from electron beam melting. Additive Manufacturing 2015;5:40-53.
[8] Ramsperger M, Mújica Roncery L, Lopez-Galilea I, Singer RF, Theisen W, Körner C. Solution Heat Treatment of the Single Crystal Nickel-Base Superalloy CMSX-4 Fabricated by Selective Electron Beam Melting. Advanced Engineering Materials 2015;17:1486-93.

[9] Ramsperger M, Singer RF, Körner C. Microstructure of the Nickel-Base Superalloy CMSX-4 Fabricated by Selective Electron Beam Melting. Metallurgical and Materials Transactions A 2016:1-12.
[10] Acharya R, Bansal R, Gambone JJ, Das S. A Coupled Thermal, Fluid Flow, and Solidification Model for the Processing of Single-Crystal Alloy CMSX-4 Through Scanning Laser Epitaxy for Turbine Engine Hot-Section Component Repair (Part I). Metallurgical and Materials Transactions B 2014;45:2247-61.
[11] Acharya R, Bansal R, Gambone JJ, Das S. A Microstructure Evolution Model for the Processing of Single-Crystal Alloy CMSX-4 Through Scanning Laser Epitaxy for Turbine Engine Hot-Section Component Repair (Part II). Metallurgical and Materials Transactions B 2014;45:2279-90.
[12] Basak A, Acharya R, Das S. Additive Manufacturing of Single-Crystal Superalloy CMSX-4 through Scanning Laser Epitaxy –Computational Modeling, Experimental Process Development, and Process Optimization. Metallurgical and Materials Transactions A (Accepted).
[13] Acharya R, Bansal R, Gambone JJ, Kaplan MA, Fuchs GE, Rudawski N, et al. Additive Manufacturing and Characterization of René 80 Superalloy Processed Through Scanning Laser Epitaxy for Turbine Engine Hot-Section Component Repair. Advanced Engineering Materials 2015;17:942-50.
[14] Acharya R, Das S. Additive Manufacturing of IN100 Superalloy Through Scanning Laser Epitaxy for Turbine Engine Hot-Section Component Repair: Process Development, Modeling, Microstructural Characterization, and Process Control. Metallurgical and Materials Transactions A 2015:1-12.